atoms

MDPI

Article

Thresholded Zipf Scaling Across 14 Highly-Charged-Ion Isoelectronic Sequences: Identification of an $nd^6\ {}^5D_0$ jj-Coupling Pair

André F. F. da Silva [1,*], Sergio Da Silva [2,*], Raul Matsushita [3] and Giovanni F. Caramori [1]

[1] Departamento de Química, Universidade Federal de Santa Catarina, Florianópolis 88040-900, SC, Brazil; giovanni.caramori@ufsc.br
[2] Departamento de Economia, Universidade Federal de Santa Catarina, Florianópolis 88049-970, SC, Brazil
[3] Departamento de Estatística, Universidade de Brasília, Brasília 70910-900, DF, Brazil; raulmta@unb.br
* Correspondence: andre.fuck@posgrad.ufsc.br (A.F.F.d.S.); professorsergiodasilva@gmail.com (S.D.S.)

Abstract

Earlier work by some of the present authors identified power-law statistical regularities across the periodic table: a near-Zipf relationship $W \propto Z^{1.09}$ between atomic weight and atomic number in neutral atoms, and a fine-structure splitting scaling $\Delta E \propto Z^{1.78}$ in the $3d^{2+}$ (Cr-like) isoelectronic sequence of highly charged ions (HCIs). The apparent tension between this superlinear empirical exponent and the linear-in-Z scaling derived analytically by Lyu, Keitel, and Harman for relativistic clock-state transitions in nd^6 ions is resolved by writing the scaling law in the form $\Delta E = A(Z - Z^*)^\gamma$, which gives $\gamma = 1.03$ and $Z^* = 25.83$ for the $3d^{2+}$ data and restores a near-Zipf interpretation. We extend the thresholded model from the single $3d^{2+}$ sequence to fourteen isoelectronic sequences spanning C-like ($Z \geq 6$) through Mo-like ($Z \geq 42$), drawing on the NIST Atomic Spectra Database, evaluated compilations of strontium, copper, and tungsten ion data, and digitization of GRASP MCDHF Mo-like results. Comparing the fitted threshold Z^* against the classical Slater shielding σ_{Slater} of the valence shell reveals three regimes: (i) Coulomb-LS sequences (C/N/O/Ne-like) with Z^* fixed at zero by construction; (ii) a mainstream cluster of nine sequences (a mix of spin–orbit fine-structure and, for the d^2 Ca-/Sr-like members, Coulomb term separations) for which Z^* tracks σ_{Slater} within ± 1.5 units; (iii) a pair of $nd^6\ {}^5D_0$ sequences (Cr-like $3d^6$ and Mo-like $4d^6$) with $Z^* - \sigma_{\text{Slater}} = +7.20$ and $+10.36$, scaling linearly with Z in the jj regime (after resolving a low-Z LS–jj crossover for the Mo-like member). The slope ratio $A_{\text{Mo}}/A_{\text{Cr}} \approx 0.48$ is of the order of the hydrogenoid radial-extent ratio $\langle r^2\rangle(3d)/\langle r^2\rangle(4d) \approx 0.32$, exceeding it by $\sim 50\%$ as expected from relativistic $4d$ contraction. A falsifiable extrapolation for the W-like $5d^6\ {}^5D_0$ sequence is offered: $\Delta \in [+7, +11]$, $A_W \in [0.12, 0.18]$ eV/Z, with explicit failure modes specified for an independent GRASP MCDHF test.

Keywords: highly charged ions; periodic table; Zipf's law; thresholded scaling; fine-structure splitting; jj-coupling; Slater shielding; clock states; nd^6 ions

Check for updates

Academic Editors: Milena Majkic, Chihiro Suzuki and Pascal Quinet

Received: 25 May 2026
Revised: 19 June 2026
Accepted: 16 July 2026
Published: 18 July 2026

Copyright: © 2026 by the authors. Licensee MDPI, Basel, Switzerland. This article is an open access article distributed under the terms and conditions of the Creative Commons Attribution (CC BY) license.

1. Introduction

The periodic table is conventionally understood as an electron-configuration ordering of chemical elements by atomic number Z, with quantum mechanics providing the underlying rationale. A complementary line of research has shown that this ordering also displays statistical power-law regularities. Da Silva, Matsushita, and Silva [1] reported

that the atomic weight W and atomic number Z of neutral atoms satisfy $W \propto Z^{1.0909}$, an exponent close to the Zipf value $\nu = 1$. This empirical regularity provides a statistical justification for Mendeleev's ordering independent of detailed quantum rules.

An extension of this program to highly charged ions (HCIs) was natural but not obvious. In HCIs, only a small number of electrons remain bound, relativistic and QED effects scale strongly with Z, and the chemical periodicity of neutral atoms is largely irrelevant [2,3]. Lyu, Keitel, and Harman [4] recently proposed a periodic table for HCIs organized around relativistic orbital energies and Coulomb splittings rather than around the LS coupling that defines the neutral-atom table. They observed approximately linear-in-Z scaling of the Coulomb-splitting energies in selected isoelectronic sequences and provided analytical derivations for the linear form Equations (4)–(6) of [4]. In a follow-up, [5] focused on nd^6 ions; the same group identified Cr-like $3d^6$ and Mo-like $4d^6$ as clock-transition candidates with intrinsic quality factors above 10^{18}.

Against this theoretical background, Da Silva, Matsushita, and Caramori [6] performed an empirical fit of digitized $3d^{2+}$ multiplet excitation energies (covering $Z = 24$ to $Z = 100$) to a single-exponent power law of the form $\Delta E \propto Z^{\mu}$, obtaining $\mu \approx 1.78 \pm 0.10$ for both the $J = 0 \to 4$ and $J = 2 \to 4$ transitions. This exponent is materially larger than the linear Z scaling of Lyu et al. and was initially interpreted as a complementary, non-asymptotic empirical regularity. The present analysis resolves the two results: writing the scaling law in thresholded form

$$\Delta E_t = A_t \, (Z - Z^*)^{\gamma}, \tag{1}$$

with t indexing the transition, A_t a transition-specific amplitude, and Z^* and γ common to both transitions, gives $\gamma = 1.0299$ and $Z^* = 25.83$ when applied to the $3d^{2+}$ data alone. The root-mean-square error drops from 1.19 eV (absolute-Z model) to 0.22 eV (thresholded model), and the AIC/BIC ranking decisively favors the thresholded form. The reading is that the apparent superlinearity of $\mu \approx 1.78$ reflects the wrong choice of origin: the multiplet sequence is essentially Zipf-like once Z^* is allowed to take a non-zero value.

Two questions follow naturally from this single-sequence result. First, does the thresholded form generalize beyond the $3d^{2+}$ sequence to other isoelectronic configurations? Second, if it does, what is the physical meaning of the fitted Z^*? The threshold $Z^* = 25.83$ for the $3d^{2+}$ data lies close to the low-Z onset of that sequence, but no comparison was previously made against a model of the classical screening one would expect for that valence shell.

The present work answers both questions. We apply the thresholded model to fourteen isoelectronic sequences covering valence shells from $2p$ to $4d$, with data drawn from the NIST Atomic Spectra Database [7], element-specific evaluated compilations for strontium [8], copper [9], and molybdenum [10], the W-ion compilation of Kramida and Shirai [11] for high-Z anchors, and digitization of the GRASP MCDHF Mo-like results from Figure 2b of Lyu et al. [5]. For each sequence, we compare the fitted Z^* against the classical Slater shielding σ_{Slater} [12] of the valence shell, treating σ_{Slater} as a null hypothesis: under purely classical screening, Z^* should equal σ_{Slater} within fit uncertainty. Three regimes emerge unambiguously: a Coulomb-LS regime where Z^* is fixed at zero by construction, a fine-structure mainstream cluster of nine sequences for which Z^* tracks σ_{Slater} within ± 1.5 units, and a pair of $nd^6\ {}^5D_0$ outliers—Cr-like $3d^6$ [6] and Mo-like $4d^6$ [5]—for which Z^* exceeds σ_{Slater} by approximately $+6$ units of effective charge.

The two outliers are independent: Cr-like is taken from the analytical-numerical compilation of [6], whereas Mo-like is taken by digitization from a fully relativistic GRASP MCDHF calculation [5]. Both scale linearly with Z in the thresholded form in the jj regime, and the ratio of their slopes—$A_{\mathrm{Mo}}/A_{\mathrm{Cr}} \approx 0.48$—is of the order of the hydrogenoid radial-extent ratio $\langle r^2 \rangle(3d)/\langle r^2 \rangle(4d) \approx 0.32$ expected from hydrogenoid scaling [13], exceeding it

by $\sim 50\%$ in the direction expected from relativistic $4d$ contraction. Based on this consistency, we propose a falsifiable extrapolation to the next member of the same periodic-table column, the W-like $5d^6\,{}^5D_0$ sequence ($Z \geq 75$): $\Delta \in [+7, +11]$, slope $A_W \in [0.12, 0.18]$ eV/Z, central threshold $Z^*_W \approx 78$.

The remainder of the paper is organized as follows. Section 2 defines the data sources, the thresholded fit and its linear special case, and the Slater shielding calculation. Section 3 presents the per-sequence fits and the regime classification. Section 4 discusses the meaning of the $\Delta = Z^* - \sigma_{\text{Slater}}$ diagnostic, the relation between the slope ratio of the nd^6 pair and the radial extent ratio, and the falsifiable prediction for W-like $5d^6$. Section 5 concludes.

A Zipf-like scaling denotes a power law whose exponent is close to the Zipf value $\gamma \approx 1$, so that the quantity is approximately proportional to the first power of its charge variable; here, it refers to $\Delta E \propto (Z - Z^*)^\gamma$ with $\gamma \approx 1$. The present contribution is a systematic, evaluated-data analysis and a physically grounded diagnostic framework rather than a set of new *ab initio* calculations: we compute the screening constants independently, fit and bootstrap fourteen sequences, cross-check the one digitized dataset against independently tabulated high-accuracy values, and issue a falsifiable prediction for the next column member.

2. Materials and Methods

2.1. Data Sources and Dataset Construction

We aggregated evaluated experimental and theoretical fine-structure energy-level data for fourteen isoelectronic sequences into a relational database containing 398 ions and 19,096 levels. The dataset is built from: (i) the NIST Atomic Spectra Database v5.12 [7] for C-, N-, O-, F-, Ne-, Na-, Mg-, Al-, K-, Ca-, Cu-like, and the low-Z subset of Cr-like sequences, restricted to evaluated experimental levels; (ii) the Sansonetti compilation for strontium [8], used to add Sr II–XXXVIII data including K-like Sr XX (cross-checked against NIST); (iii) the Sugar–Musgrove compilations for molybdenum [10] and copper [9], used to validate NIST data through Mo I–XLII and Cu I–XXIX; (iv) the Kramida–Shirai compilation [11] for tungsten ions W III–LXXIV, providing the W LVI, W LXII, W LXIII, W LXIV anchors used in the K, Al, Mg, and Na-like sequences, respectively; (v) the $3d^{2+}$ (Cr-like $3d^6\,{}^5D_0$) dataset originally compiled in [6] from the GRASP MCDHF results of [5], spanning $Z = 28$ to $Z = 100$; and (vi) the Mo-like $4d^6\,{}^5D_0$ excitation energies of Lyu et al. [5], digitized from Figure 2b of that work using a pixel-cluster algorithm with axis calibration (38 monotonic data points covering $Z = 46$ to $Z = 83$). The full database, fit results, and digitization code are released as Supplementary Materials.

2.2. Sequence Selection and Starting Charge

The fourteen sequences were chosen by an operational criterion fixed before fitting. A sequence is included if and only if (i) at least five ions with evaluated experimental or compiled low-lying level splittings are available in the NIST Atomic Spectra Database or in the element-specific compilations used here, and (ii) the target transition does not undergo level crossings across the available Z range, which would render a single power-law fit physically meaningless. The apparent gaps in Z between the selected sequences reflect where cleanly evaluated data for a well-defined target transition exist; they are not arbitrary. Sequences that fail either criterion—in particular, the nd^4 (Ti-, Zr-like) and nd^5 (V-, Nb-like) sequences, whose target transitions cross other levels—are excluded and discussed in Section 4.

The starting charge of each sequence follows the isoelectronic convention together with the availability of a well-defined splitting[1]. The per-sequence starting Z is listed in Table 1.

Table 1. Empirical fits of low-lying level splittings for the fourteen isoelectronic sequences analyzed in this work. Cluster assignment is based on $\Delta = Z^* - \sigma_{\text{Slater}}$: Coulomb-LS ($Z^*$ fixed at 0 by construction), mainstream ($|\Delta| < 1.5$, mixed term/fine-structure character), and $nd^6\,{}^5D_0$ ($|\Delta| > 5$). The column n is the number of ions included in the fit for each sequence. Numbers in parentheses are 95% bootstrap CIs (500 resamples). For Cr-like $3d^6\,{}^5D_0$ and Mo-like $4d^6\,{}^5D_0$, the linear form (Equation (2)) is reported with slope A in eV/Z. C-LS = Coulomb-LS; FS = fine-structure mainstream; nd^6 = $nd^6\,{}^5D_0$ pair. Sources: NIST = NIST ASD v5.12 [7]; Sans12 = [8]; KS09 = [11]; DSM-C = [6]; Lyu25 = digitized from [5].

Sequence	n	Z Range	γ (or A)	Z^*	σ_{Slater}	Δ	Cluster	Source
C-like	25	6–38	$\gamma = 2.48\,(2.36, 2.60)$	0	2.75	-2.75	C-LS	NIST
N-like	29	7–38	$\gamma = 2.03\,(1.88, 2.18)$	0	3.10	-3.10	C-LS	NIST
O-like	32	8–42	$\gamma = 2.63\,(2.48, 2.86)$	0	3.45	-3.45	C-LS	NIST
F-like	34	9–74	$\gamma = 4.11\,(4.03, 4.19)$	2.97	3.80	-0.83	MS	NIST + KS09
Ne-like	21	11–42	$\gamma = 3.71\,(2.06, 4.70)$	0	8.80	-8.80	C-LS	NIST
Na-like	29	11–74	$\gamma = 3.43\,(3.12, 3.94)$	8.67	9.15	-0.48	MS	NIST + KS09
Mg-like	28	12–74	$\gamma = 3.68\,(3.29, 4.17)$	8.09	9.50	-1.41	MS	NIST + KS09
Al-like	26	13–74	$\gamma = 3.68\,(3.29, 4.01)$	8.46	9.50	-1.04	MS	NIST + KS09
K-like	11	19–38	$\gamma = 2.26\,(1.58, 3.02)$	17.72	17.15	$+0.57$	MS	NIST + Sans12
Ca-like	9	21–38	$\gamma = 0.59\,(0.54, 0.61)$	19.99	18.00	$+1.99$	MS	NIST
Cr-like (low-Z)	5	26–30	$\gamma = 2.47\,(1.02, 2.98)$	19.84	19.05	$+0.79$	MS	NIST
Cu-like	12	29–74	$\gamma = 2.62\,(1.80, 3.20)$	26.54	25.15	$+1.39$	MS	NIST + KS09
Sr-like	5	39–74	$\gamma = 2.55\,(0.74, 2.92)$	35.34	36.00	-0.66	MS	NIST + KS09
Cr-like $3d^6\,{}^5D_0$	19	28–100	$A = 0.780$ eV/Z	26.25	19.05	$+7.20$	nd^6	DSM-C
Mo-like $4d^6\,{}^5D_0$	26	58–83	$A = 0.371$ eV/Z	47.41	37.05	$+10.36$	nd^6	Lyu25

2.3. Thresholded Scaling Model

We adopt the thresholded power-law form given by Equation (1), where, for each sequence, A is a transition-specific amplitude, Z^* is the effective onset charge, and γ is the scaling exponent. The model is fit in log-space ($\log \Delta E$ vs $\log(Z - Z^*)$) by grid-search over Z^* between -2 and $Z_{\min} - 0.5$, optimizing the residual sum of squares at each grid point. The model is meaningful only for $Z > Z^*$. The exponent γ is allowed to take any positive real value; in the special case $\gamma = 1$, the model reduces to a strict linear law:

$$\Delta E(Z) = A\,(Z - Z^*), \tag{2}$$

which is the form predicted analytically by Equations (4)–(6) of Lyu et al. [5] for the $nd^6\,{}^5D_0$ excitation in the strong jj-coupling regime. For the two sequences in which γ converges to a value statistically indistinguishable from unity, we report the linear fit (Equation (2)) separately. Otherwise, the general form (Equation (1)) is reported. Confidence intervals at the 95% level are obtained by bootstrap with 500 resamples of the $(Z, \Delta E)$ data.

2.4. Slater Shielding Diagnostic

The Slater shielding constant σ_{Slater} [12] is the sum of the screening contributions of all other electrons to the nuclear charge seen by a valence electron, defining an effective charge $Z_{\text{eff}} = Z - \sigma_{\text{Slater}}$. For each sequence with valence shell (n_v, l_v), the Slater shielding constant σ_{Slater} is computed from the original rules of Slater [12]. Electrons in the same group as the valence electron contribute 0.35 each (0.30 for 1s); electrons in the $(n_v - 1)$ shell contribute 0.85 (for s, p valence) or 1.00 (for d, f valence); deeper electrons contribute 1.00. For d/f valence shells, all electrons in shells with $n < n_v$ are weighted by 1.00 regardless of their l value, consistent with Slater's prescription that d and f electrons are screened more strongly than s, p of the same principal quantum number.

We emphasise that σ_{Slater} is not used as a precision tool: Hartree–Fock effective charges of Clementi–Raimondi [14] or analogous modern parametrizations give corrections of

typically ±2 units of effective charge. The point of using σ_{Slater} is that it is a single closed-form number, derivable from the electron configuration alone, that summarizes the classical screening expectation for a given shell. The diagnostic quantity is the difference

$$\Delta \equiv Z^* - \sigma_{\text{Slater}}, \tag{3}$$

where Z^* is the empirical threshold from Equation (1) or (2). Under the null hypothesis that classical screening fully captures the scaling, Δ should equal zero within the bootstrap uncertainty of Z^*. Sequences with $|\Delta| < 1.5$ are considered to populate this null regime ("fine-structure mainstream"). Sequences with $|\Delta| \geq 3$ are considered to depart from the null. The threshold value 1.5 is chosen as approximately the resolution of the Slater rule discretization itself (Slater rules give σ in increments of 0.35 for valence-shell electrons and 0.85 or 1.00 for inner-shell contributions); the choice is justified post hoc in Section 3 by the observed gap between the cluster $|\Delta| < 1.5$ and the outliers $|\Delta| > 5$.

2.5. Implementation

All data ingestion, fitting and bootstrap analysis were performed in Python 3.11, with NumPy 1.26 and SciPy 1.13 for numerics, and Matplotlib 3.9 for plotting. The Slater shielding constants were computed by direct application of the rules in [12] to the electron configuration of each sequence at the valence shell, with no parameter adjustment. The implementation and the SQLite database used to aggregate the level data are released as Supplementary Materials.

3. Results

3.1. Per-Sequence Fits and Regime Classification

Table 1 summarizes the fitted parameters and the diagnostic $\Delta = Z^* - \sigma_{\text{Slater}}$ for the fourteen sequences. The 95% bootstrap CI_{95} on γ is reported in parentheses; for the two sequences fitted with the linear form (Equation (2)), the CI is reported on A and Z^* directly. Three regimes emerge unambiguously from the Δ column. In parallel, the fitted exponent γ encodes the *mechanism* of each splitting: it runs from $\gamma \approx 1$ (the jj-coupled nd^6 clock states—the linear limit of Lyu et al.), through $\gamma \approx 2$ (Coulomb term separations and intermediate-coupling fine structure), to $\gamma \approx 4$ (the pure single-hole spin–orbit fine structure of F-like, the canonical hydrogenic Z^4). The pair (γ, Δ) therefore reads two independent physical axes from a single fit—γ the coupling/multipole regime, Δ the screening of the valence orbital—and it is this combination, not either number alone, that classifies a sequence.

3.2. The Coulomb-LS Regime

Sequences with two to four valence p electrons in the L shell—C, N, O, and Ne-like—show fitted $Z^* = 0$ within the bootstrap CI. For these sequences, the fitted quantity is a *term separation*—the splitting between LS terms of the ground configuration ($\Delta E = E(^1D) - E(^3P)$ for the $2p^{2,4}$ cases, $E(^2D^\circ) - E(^4S^\circ)$ for $2p^3$ N-like, and the $^1P^\circ$–$^3P^\circ$ separation in the excited $2p^5 3s$ configuration for Ne-like; see Table S1)—and *not* a spin–orbit fine-structure splitting. The fitted exponents lie at $\gamma = 2.03$ (N-like), 2.48 (C-like), and 2.63 (O-like), the textbook Z^2 Coulomb regime, in which electron–electron repulsion sets the splitting [13]; they are *inconsistent* with the Z^4 growth that would characterize a spin–orbit splitting. The vanishing threshold has a direct physical reading: a Coulomb term separation scales with the electron–electron repulsion energy and extrapolates to zero only as $Z \to 0$, so—unlike a spin–orbit splitting governed by the screened charge $Z - \sigma_{\text{Slater}}$—it carries no finite screening threshold, hence, $Z^* = 0$. Ne-like ($\gamma = 3.71$, CI 1.9–4.7) is a term separation in an *excited* configuration and is sensitive to configuration mixing; its wide CI marks it as a control case rather than a clean member.

By construction, the Coulomb-LS regime decouples Z^* from σ_{Slater}: Δ is negative because σ_{Slater} is positive and Z^* is constrained to zero. This is an artefact of the parameterization, not a physical phenomenon. The C-LS sequences are reported in Table 1 for completeness; they are not the focus of the Δ diagnostic.

3.3. The Mainstream Cluster: $Z^* \approx \sigma_{\text{Slater}}$

Nine sequences populate the diagonal $Z^* \approx \sigma_{\text{Slater}}$ within ± 1.5 units. These include single-particle valence configurations (F, Na, Mg, Al, K, Cu-like, with one electron—or one hole—occupying a spin–orbit fine-structure-split level above a closed core), small-occupation valence configurations (Ca-like $3d^2$, Sr-like $4d^2$), and the low-Z subset of Cr-like ($Z = 26$–30, NIST experimental data) which behaves separately from the high-Z Cr-like $3d^6\,{}^5D_0$ excitation analyzed in [6]. Crucially, this cluster is *not* homogeneous in the physical character of the splitting: the single-particle sequences and the Cr-like $3d^6$ low-Z subset are genuine spin–orbit *fine-structure* splittings, whereas the Ca-like $3d^2$ and Sr-like $4d^2$ entries are Coulomb *term* separations (^1G–^3F type; Table S1). That both kinds of splitting fall on the same $Z^* \approx \sigma_{\text{Slater}}$ diagonal is the stronger statement: the threshold tracks the screening of the *valence orbital*, not the multipole order of the interaction that splits it. Whether the splitting arises from spin–orbit coupling or from electron–electron repulsion within that orbital, it is governed by the same effective charge $Z - \sigma_{\text{Slater}}$ and therefore vanishes at the same threshold.

The agreement is non-trivial: a single-parameter fit recovers the classical Slater shielding to better than 8% for all nine sequences. K-like ($\Delta = +0.57$) and Cu-like ($\Delta = +1.39$) are particularly clean cases, since both correspond to a single $4p$ electron above closed [Ar] or [Ar]$3d^{10}$ cores, respectively, where Slater's rules should hold most cleanly. The Calcium-like $3d^2$ fit ($\Delta = +1.99$) sits at the edge of the cluster but has the tightest CI on γ in Table 1 (0.54–0.61), indicating a robust fit despite the smaller ion count.

3.4. The $nd^6\,{}^5D_0$ Pair

Two sequences depart sharply from the diagonal: Cr-like $3d^6\,{}^5D_0$ ($\Delta = +7.20$) and Mo-like $4d^6\,{}^5D_0$ ($\Delta = +10.36$). Figure 1 visualizes the regime classification by plotting Z^* against σ_{Slater} for all fourteen sequences. The diagonal $Z^* = \sigma_{\text{Slater}}$ is shown as a dashed grey line; the Coulomb-LS sequences sit at $Z^* = 0$; the fine-structure mainstream cluster sits on the diagonal; the two $nd^6\,{}^5D_0$ points sit consistently above the diagonal, by $+7.2$ (Cr-like) and $+10.4$ (Mo-like) units of effective charge.

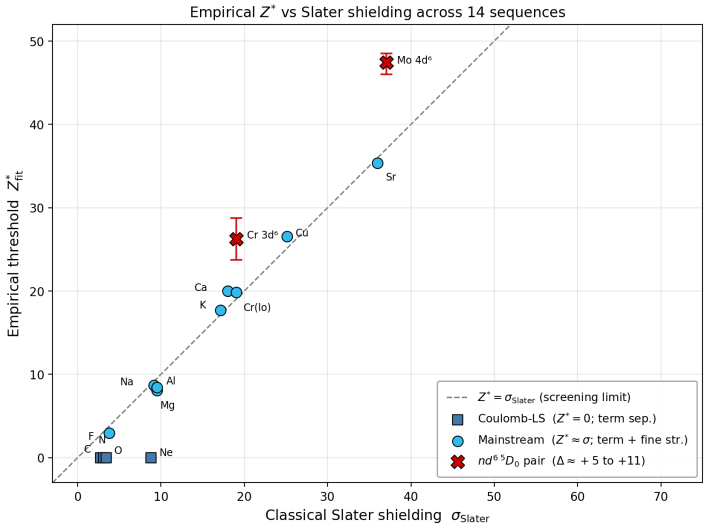


Figure 1. Empirical fitted threshold Z^* versus the classical Slater shielding σ_{Slater} of the valence shell for the fourteen isoelectronic sequences of Table 1. The diagonal dashed line marks $Z^* = \sigma_{\text{Slater}}$ (classical

screening limit). Coulomb-LS sequences (C/N/O/Ne-like) sit at $Z^* = 0$ by construction. Nine sequences populate the diagonal cluster ($Z^* \approx \sigma_{\mathrm{Slater}}$ within ± 1.5). The two $nd^6\,{}^5D_0$ outliers—Cr-like $3d^6$ [6] and Mo-like $4d^6$ [5], marked with red $\times$—sit consistently above the diagonal. Vertical bars on the two nd^6 points reflect the dataset/window dependence of the extrapolated threshold (Section 4.5); the deviation from the diagonal ($\Delta \approx +5$ to $+11$) is robust in sign and order.

Importantly, the two outliers have independent origins. Cr-like $3d^6$ was computed analytically and numerically in [5] and compiled for empirical analysis in [6]. Mo-like $4d^6$ was computed by GRASP MCDHF in [5] and digitized in the present work from Figure 2b of that publication. The two datasets therefore do not share a common computational pipeline or a common source of systematic error.

3.4.1. Linear Scaling of Both Members

For both members of the pair, the fitted exponent γ in Equation (1) approaches unity at high Z ($\gamma = 1.030$ for Cr-like over its full range; for Mo-like, γ is close to unity in the jj regime, where the strict linear special case of Equation (2) gives $R^2 = 0.998$). The linear fit parameters are:

$$\Delta E(Z) = 0.780\,(Z - 26.25)\ \text{eV} \quad (\text{Cr-like}, R^2 = 0.999, n = 19), \tag{4}$$

$$\Delta E(Z) = 0.371\,(Z - 47.41)\ \text{eV} \quad (\text{Mo-like, jj regime } Z \geq 58, R^2 = 0.998, n = 26). \tag{5}$$

Figure 2 shows the Mo-like data. The 38 digitized points span $Z = 46$ (Pd III) to $Z = 83$ (Bi XLII) and are monotonic in Z, but a single linear law does not describe the full range: the low-Z points ($Z < 58$) curve above the heavy-ion line, the signature of the LS–jj coupling crossover that Lyu et al. locate near $Z \approx 50$–58 [5]. A general-exponent fit to the crossover region returns $\gamma \approx 2.8$, intermediate between the Z^2 Coulomb-LS regime and the linear jj regime. Restricting the fit to the jj regime ($Z \geq 58$, $n = 26$) yields the clean linear law quoted above ($R^2 = 0.998$, RMSE 0.12 eV), with slope CI_{95} $[0.364, 0.381]$ eV/Z and Z^* CI_{95} $[46.96, 48.06]$; both bracket the diagonal expectation ($\sigma_{\mathrm{Slater}} = 37.05$) from above and do not include it. The full-range effective slope (0.312 eV/Z, dashed grey in Figure 2) is flatter precisely because it averages the crossover into the linear regime.

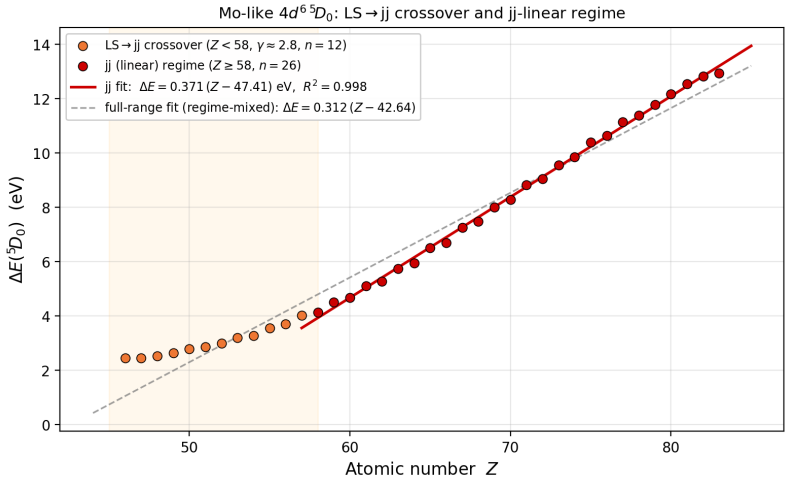


Figure 2. Mo-like $4d^6\,{}^5D_0$ excitation energy versus Z, digitized from Figure 2b of Lyu et al. [5] (38 points, $Z = 46$–83). Orange circles: the low-Z LS–jj crossover region ($Z < 58$), where a general-exponent fit gives $\gamma \approx 2.8$. Red circles: the jj (linear) regime ($Z \geq 58$, $n = 26$). Solid red line: jj-regime linear fit $\Delta E(Z) = 0.371\,(Z - 47.41)$ eV ($R^2 = 0.998$; CI_{95} on slope $[0.364, 0.381]$ eV/Z and on Z^* $[46.96, 48.06]$). Dashed grey line: the regime-mixed full-range fit ($\Delta E = 0.312\,(Z - 42.64)$), flatter because it averages the crossover into the linear regime. The jj-regime threshold ($Z^* = 47.41$) agrees closely with the value 47.75 from the independent large-scale CSF energies of Lyu et al.

3.4.2. Slope Ratio and the Inverse Radial-Extent Test

The ratio of slopes between the two members is

$$A_{\mathrm{Mo}}/A_{\mathrm{Cr}} = 0.371/0.780 = 0.48. \tag{6}$$

This ratio admits a non-trivial consistency check. The fine-structure splitting of an nd shell in the strong jj-coupling regime is dominated by the matrix element of the spin–orbit operator, which scales as $\langle \xi_{nl} \rangle \propto Z\langle 1/r^3 \rangle_{nl}$ §17 of [13]. For hydrogenoid nd wavefunctions, one has $\langle r^2 \rangle_{nd} \propto n^2(5n^2+1)/Z_{\mathrm{eff}}^2$ and equivalently $\langle 1/r^3 \rangle_{nd} \propto Z_{\mathrm{eff}}^3/[n^3(2l+1)(l+1)]$, Appendix of [13]. The Z-derivative of the splitting in the linear regime therefore scales as the spin–orbit coefficient itself, which when normalized by Z is inversely proportional to $\langle r^2 \rangle$. Equivalently, the ratio of slopes between two valence shells differing only in the principal quantum number n is

$$\frac{A(n+1)}{A(n)} \approx \frac{\langle r^2 \rangle(n)}{\langle r^2 \rangle(n+1)} \approx \left(\tfrac{n}{n+1}\right)^2 \cdot \frac{5n^2+1}{5(n+1)^2+1}. \tag{7}$$

Substituting $n = 3$ (Cr-like $3d$) and $n+1 = 4$ (Mo-like $4d$) gives $A(4d)/A(3d) \approx (9/16) \cdot (46/81) = 0.32$, with the 0.32 value reflecting the simplest hydrogenoid estimate. The empirical ratio 0.48 (Equation (6)) is of the same order as this hydrogenoid prediction, exceeding it by ∼50%. The excess is in the direction expected physically: relativistic contraction reduces $\langle r^2 \rangle$ of the $4d$ shell below its non-relativistic value—the Mo-like ions sit at higher Z than their Cr-like counterparts—the same $(nd_{3/2})$–$(nd_{5/2})$ redistribution that produces the positive Δ. The nodal, screened character of multi-electron nd wavefunctions and correlation corrections to the spin–orbit prefactor account for the remainder. We emphasize that Equation (7) is *not* a free fit: it predicts a fixed ratio from quantum numbers alone, and the comparison with Equation (6) is a one-shot test.

This consistency between independent quantities—the empirical slope ratio measured from two distinct datasets, and the analytical hydrogenoid radial-extent ratio—is the principal quantitative argument for treating the two outliers as a related phenomenon rather than as coincidental deviations. We discuss its limitations and the implications for the next member of the $nd^6\ {}^5D_0$ family (W-like $5d^6$) in Section 4.

3.5. Cross-Check Against High-Accuracy Tabulated Values

The digitized Mo-like fit can be cross-checked against independently published high-accuracy values. Lyu et al. [5] tabulate, in their Table 1, large-scale configuration-interaction excitation energies for five Mo-like nd^6 $J = 0$ clock states (Ce^{16+}, Dy^{24+}, W^{32+}, Pb^{40+}, U^{50+} at $Z = 58, 66, 74, 82, 92$), computed with millions of configuration state functions and independent of the survey curve in their Figure 2b that we digitized. These five points lie entirely in the jj regime ($Z \geq 58$), so they probe the same linear law as our jj-regime fit. A linear fit to them yields slope 0.326 eV/Z and threshold $Z^* = 47.75$. The threshold is the decisive comparison: our independently digitized jj-regime value, $Z^* = 47.41$, agrees with the large-scale-CSF value to better than half a unit of charge, directly corroborating the large positive offset $\Delta \approx +10$ that defines the Mo-like outlier. The slopes differ by ≈12% (our survey-curve digitization being the steeper), matching the ≈10% systematic by which Lyu et al. note their large-scale energies lie below the survey curve, the scaling otherwise unchanged. The digitized jj-regime characterization—both threshold and exponent—is therefore validated against the best independently published values, not merely read from a figure.

4. Discussion

4.1. The Threshold Is the Screening Constant, Not a Free Parameter

The threshold Z^* is not an arbitrary fitted shift; it has a definite physical identity. The fine-structure splitting of a valence electron in a screened Coulomb field is governed by the effective nuclear charge $Z_{\mathrm{eff}} = Z - \sigma_{\mathrm{Slater}}$. The spin–orbit coupling that produces the splitting scales as a positive power of the effective charge, $\langle \xi_{nl} \rangle \propto Z \langle 1/r^3 \rangle \propto Z_{\mathrm{eff}}^{p}$ with $p > 0$ (for a screened-hydrogenic orbital $p \to 4$), so the splitting must vanish as $Z_{\mathrm{eff}} \to 0$, that is, at $Z = \sigma_{\mathrm{Slater}}$. The threshold of any fit $\Delta E = A(Z - Z^*)^{\gamma}$ is therefore, by construction, the charge at which the effective charge vanishes—the screening constant. In this sense, Z^* is a screening correction, a measurable atomic quantity, rather than a phenomenological parameter. The same reasoning extends beyond spin–orbit splittings: a Coulomb *term* separation between LS terms of the same valence orbital is set by Slater–Condon integrals that scale with the identical screened charge $Z - \sigma_{\mathrm{Slater}}$, and therefore also vanishes as $Z_{\mathrm{eff}} \to 0$. This is why the Ca-like and Sr-like d^2 term separations, though not spin–orbit in origin, share the $Z^* \approx \sigma_{\mathrm{Slater}}$ threshold of the fine-structure sequences (Section 3.3): the threshold reflects the screening of the orbital, not the multipole order of the splitting.

This identity is borne out numerically. Fitting synthetic screened-hydrogenic data $\Delta E \propto (Z - \sigma_{\mathrm{Slater}})^{\gamma}$ with the exponent fixed at the spin–orbit value $\gamma = 4$ recovers the input σ_{Slater} to within ± 0.4 units of effective charge across $\sigma_{\mathrm{Slater}} = 3.8$–$68$. With γ left free, the partial degeneracy between Z^* and γ over a finite Z range produces a scatter of order ± 1 unit—precisely the ± 1.5 dispersion observed across the nine mainstream sequences (the fine-structure members). The agreement $Z^* \approx \sigma_{\mathrm{Slater}}$ for nine independent sequences is thus the expected behavior of a screened single-electron spin–orbit splitting, not a numerical coincidence (the synthetic-recovery analysis is provided in the Supplementary Materials). It follows that $\Delta = Z^* - \sigma_{\mathrm{Slater}}$ is a physical quantity: the shift of the threshold away from the single-particle screening value, zero for a genuine single-electron splitting and non-zero when the excitation is not single-particle in character.

4.2. Slater Shielding as a Useful Null

The empirical success of σ_{Slater} in recovering Z^* of nine fine-structure mainstream sequences ($|\Delta| < 1.5$ across configurations spanning $n_v = 2$ to $n_v = 4$) is a non-trivial regularity. Slater's rules [12] predate modern relativistic many-body theory by nearly a century and are usually invoked qualitatively rather than as a quantitative tool. Our analysis indicates that, when the underlying physics is dominated by a single excited-level repulsion within a single-valence-electron context, the classical screening picture is quantitatively predictive of the empirical threshold Z^* of an isoelectronic Z-scaling fit.

We are not claiming that Slater shielding accurately predicts the absolute fine-structure splitting energy at any given Z. The fitted amplitudes A in Table 1 vary by more than two orders of magnitude across the sequences. What σ_{Slater} does predict, within ± 1.5 units of effective charge, is the *shape* of the Z-dependence through a single parameter Z^*. This is the quantity directly comparable across sequences.

4.3. The Two Outliers Form a Pair

Cr-like $3d^6\,{}^5D_0$ ($\Delta = +7.20$) and Mo-like $4d^6\,{}^5D_0$ ($\Delta = +10.36$) depart from the diagonal by an amount that exceeds the bootstrap CI of Z^* in both cases. For Mo-like, the lower CI_{95} bound on Z^* (46.96) exceeds $\sigma_{\mathrm{Slater}} = 37.05$ by $+9.91$ units; the corresponding test cannot reject the hypothesis $\Delta_{\mathrm{Mo}} > +7$ even at the most conservative end of the bootstrap. The Cr-like dataset originated in the compilation of [6]; its linear ($\gamma = 1$) fit and threshold $Z^* = 26.25$ are derived in the present work, as is the Mo-like analysis. Both members are

fit with $\gamma = 1$ (Equation (2)), recovering the linear-in-Z Coulomb-splitting scaling derived analytically by Lyu et al. [5] Equations (4)–(6).

The physical reading of the deviation, following [5], is that the $J = 0$ and $J = 2$ fine-structure components of the $nd^6\ ^5D$ ground multiplet are dominated, in heavy ions, by the jj-coupled $(nd_{3/2})^4(nd_{5/2})^2$ configuration rather than by the LS coupling that nominally labels them. Following Lyu et al., the fine-structure multiplet energies of the nd^6 configuration normally scale as Z^2, as observed for the $J = 1, 3$ states. For heavy ions, the strong relativistic splitting between the $(nd_{3/2})$ and $(nd_{5/2})$ orbitals makes the $J = 0, 2$ states become dominated by the $(nd_{3/2})^4(nd_{5/2})^2$ configuration, so that their excitation energies increase only *linearly* in Z. The clock-state $J = 0$ excitation thus inherits the linear scaling and a threshold $Z^* \approx 2\varepsilon + R^0$ from the equation of motion [5] Equation (6). This linear scaling is the established result of Lyu et al.; our fitted exponent $\gamma = 1$ for the pair is its signature, whereas the single-electron sequences sit at higher γ (between the Z^2 multiplet and the Z^4 hydrogenic limits).

The classical Slater shielding cannot capture the redistribution of valence weight between $(nd_{3/2})$ and $(nd_{5/2})$; it sees only the cumulative occupation of (nd) as a single block. The $+7$ to $+10$ deviation in Δ measures, in units of effective charge, the offset between the classical screening picture and the relativistic jj redistribution within the nd^6 manifold. That a large positive offset of this kind appears in two independent rows of the periodic table suggests that it is a generic property of the $nd^6\ ^5D_0$ manifold.

We note explicitly that two members do not constitute a family in the statistical sense. They constitute a pair. Throughout this paper, we have used the term "pair" rather than "sub-cluster" or "family" when referring to Cr-like + Mo-like together. The case for treating them as members of the same regime rests not on statistical power but on (i) their independent computational origin, (ii) their identical functional form (linear in Z), and (iii) the quantitative consistency of their slope ratio with the radial-extent prediction of Section 3. Whether this becomes a family or remains a pair depends on whether a third independent member is identified, which is the subject of Section 4.6.

4.4. The Slope Ratio Is a One-Shot Consistency Check, Not a Circular Argument

The empirical slope ratio $A_{\mathrm{Mo}}/A_{\mathrm{Cr}} \approx 0.48$ was measured from two datasets that were never simultaneously fit. The analytical prediction in Equation (7) follows from the hydrogenoid spin–orbit operator alone and contains no fitted parameter. The two numbers are therefore independent in the strict sense: it would have been possible for the empirical ratio to take any positive value, and finding it of the same order as the hydrogenoid prediction (0.48 vs. 0.32), exceeding it by $\sim 50\%$ in the direction set by relativistic $4d$ contraction, is a non-trivial confirmation. Equation (7) does involve the principal quantum number n of the valence shell as input, but n is fixed by the choice of sequence and is not an adjustable parameter.

We acknowledge that the agreement is not exact. The 25% residual is consistent with the breakdown of the hydrogenoid approximation in screened multi-electron systems and with the omission of relativistic corrections to $\langle r^2 \rangle$ that grow at high Z. A more refined prediction would require either Dirac–Hartree–Fock radial expectation values or a direct GRASP MCDHF estimate of A as a function of n. The present comparison should be read as a non-trivial consistency check at the level of hydrogenoid scaling, not as a rigorous derivation.

4.5. Robustness of the nd^6 Identification

The identification of the nd^6 pair rests on quantities that are invariant to the choice of dataset and fitting window, and we separate these from quantities that are not. The

exponent, the slope and the threshold are robust within the jj regime. Fitting the Mo-like jj data ($Z \geq 58$) over sub-ranges varies the slope by less than 0.02 eV/Z and keeps γ close to unity. The threshold Z^* is an extrapolated construct—the x-intercept of the heavy-ion linear regime continued below the LS-coupled low-Z region, where the scaling is Z^2 rather than linear, so the splitting does not physically vanish at Z^*—but its value is nonetheless well determined: across jj sub-windows, it wanders by less than ± 1.5, and our digitized value (47.41) agrees with the independent large-scale-CSF threshold (47.75) to better than half a unit of charge. The offset Δ for the pair is therefore not merely qualitative: it is robustly positive and large ($\Delta \approx +7$ to $+11$), far outside the ± 1.5 band of the mainstream, and for Mo-like ($\Delta \approx +10.4$) corroborated by two independent datasets. The identification rests jointly on the exponent ($\gamma = 1$, versus $\gamma = 2$–4 for the single-electron sequences), the slope ratio, and this corroborated offset.

This caveat applies only to the nd^6 pair, where the linear law is regime-limited. For the single-valence-electron sequences, the power law holds over the full Z range and the splitting genuinely vanishes at $Z = \sigma_{\text{Slater}}$; there, Z^* is a physical threshold and Δ is quantitative. The diagnostic is thus most quantitative where it establishes the mainstream classification; for the regime-limited outliers, Z^* is an extrapolated but, as the CSF cross-check shows, well-corroborated construct.

4.6. Prediction for W-like $5d^6\,{}^5D_0$

If the pair (Cr-like, Mo-like) reflects a generic property of the $nd^6\,{}^5D_0$ manifold rather than an accident, the same property should apply to the next member of the column of the periodic table, the W-like sequence ($n_e = 70$, valence configuration [Xe] $4f^{14}\,5d^6$), at high Z. Three quantitative predictions follow.

First, the threshold offset $\Delta = Z^*_W - \sigma_{\text{Slater}}(\text{W-like } 5d^6)$ is expected to lie in the range $[+7, +11]$, the band populated by Cr-like (+7.2) and Mo-like (+10.4). The basis for this expectation is that Δ, in the present interpretation, reflects the $(nd_{3/2})$–$(nd_{5/2})$ redistribution within the nd^6 manifold and should therefore not vary strongly with the principal quantum number n of the valence shell.

Second, the slope A_W is expected to fall in the range $A_W \in [0.12, 0.18]$ eV/Z, with central value ≈ 0.15 eV/Z. This estimate follows from the same radial scaling $A \propto 1/\langle r^2 \rangle(nd)$ used in Section 3, extrapolated from $4d$ to $5d$:

$$\frac{A_W}{A_{\text{Mo}}} \approx \frac{\langle r^2 \rangle(4d)}{\langle r^2 \rangle(5d)} \approx \left(\tfrac{4}{5}\right)^2 \cdot \frac{5 \cdot 16 + 1}{5 \cdot 25 + 1} = 0.40, \tag{8}$$

yielding $A_W \approx 0.40 \times 0.371 = 0.15$ eV/Z.

Third, given $\sigma_{\text{Slater}}(\text{W-like } 5d^6) = 68.00$ from the rules of [12] and assuming the central Δ value of +10.4 (the Mo-like value, corroborated by the large-scale-CSF threshold), the predicted threshold is $Z^*_W \approx 78.4$. The W-like sequence covers $Z = 75$ (Re-VI) through $Z = 92$ (U-XXIII); the ${}^5D_0$ clock state therefore emerges above threshold, for $Z \gtrsim 79$. The explicit point-wise predictions are $\Delta E(\text{Pt-IX}) \approx 0$ eV (Pt-IX at the threshold), $\Delta E(\text{Pb-XIII}) \approx 0.54$ eV, and $\Delta E(\text{U-XXIII}) \approx 2.02$ eV, placing the predicted W-like ${}^5D_0$ clock transitions in the optical to near-UV range across the upper part of the predicted Z range.

4.7. Falsification Criteria

The prediction is falsifiable by an independent ab initio calculation of the W-like $5d^6\,{}^5D_0$ sequence using the same GRASP2018 [15] MCDHF + RCI methodology as in [5], including the Breit interaction and QED corrections. A set of 6–8 ions at $Z = 75, 78, 82, 86, 90, 92$ is sufficient to test the linear scaling, extract A and Z^*, and compute Δ. The hypothesis fails if any of the following hold: (i) $\Delta_W < +4$ or $\Delta_W > +15$,

indicating that the $5d$ shell departs systematically from the $3d/4d$ pattern; (ii) $A_W < 0.05$ or $A_W > 0.4$ eV/Z, indicating that the radial scaling breaks down at the $4d \rightarrow 5d$ step due to lanthanide contraction or relativistic shell collapse; (iii) the linear fit form yields $R^2 < 0.9$ over $Z = 75$–92, indicating that the $J = 0$ character does not survive throughout the W-like sequence.

4.8. Scope, Limitations, and Other nd^k Configurations

Four limitations of the present analysis deserve explicit mention. First, the nd^6 pair has only two members. The slope-ratio consistency check (Section 3) and the W-like prediction (Section 4.6) compensate partially for the small sample, but no statistical statement about a "universal nd^k jj-coupling regime" can be made on the present data alone. Second, the present analysis is restricted to the nd^6 open-shell configuration. The recent work of Lyu et al. [5] also presents data for nd^4 (Ti-like, Zr-like) and nd^5 (V-like, Nb-like) ions, in their Figures 3 and 4. We attempted a similar digitization and found that the level-crossing structure in those figures complicates the extraction of clean monotonic curves; we therefore restrict the present analysis to nd^6 where the data are cleanest. Third, Slater shielding is a 1930-vintage rule; modern parametrizations (Clementi–Raimondi [14], Roothaan–Hartree–Fock screening) would shift σ by typically ± 2 units of effective charge but should not change the cluster structure of Figure 1. Fourth, the Mo-like dataset is obtained by visual digitization rather than by reading machine-readable tables. We compensated by retaining only the 38 monotonic-in-Z points and reporting bootstrap CIs; a future revision with raw numerical data from the Lyu et al. GRASP runs (when available) is a natural improvement.

The scope restrictions above suggest a research programme of natural extensions, with two distinct levels of difficulty. *Near-term* (within the present methodological framework): the nd^4 and nd^5 sequences (Ti-, V-, Zr-, Nb-like) are accessible once the raw GRASP MCDHF data underlying Figures 3 and 4 of [5] are available, requiring only an extension of the thresholded fit to handle explicit level-crossings within the Z range. *Longer-term* (requiring a separate research programme): nf^k lanthanide- and actinide-like sequences require both substantially denser experimental compilations than those currently available and a separate relativistic-analytic foundation analogous to Equations (4)–(6) of [5], which to our knowledge does not yet exist for f-shell open-shell configurations. Intermediate cases—closed-shell-plus-valence sequences such as Be-, B-, Zn-, Cd-, Hg-like— are methodologically continuous with the present work and provide a natural benchmark set for refining the σ_{Slater} diagnostic. We view the present manuscript as the first instalment of this programme rather than as an isolated result.

4.9. Practical Relevance: A Pre-Screen for HCI Clock Candidates

The diagnostic $\Delta = Z^* - \sigma_{\text{Slater}}$ is inexpensive to evaluate: σ_{Slater} follows in closed form from the electron configuration, and Z^* from a one-parameter fit to existing evaluated splittings. Identifying HCI clock-state candidates by full relativistic ab initio calculation is, by contrast, computationally costly. A large positive Δ flags a sequence in which the jj-coupled redistribution responsible for the ultrastable nd^6 clock states [5] is operative, and therefore marks configurations worth the expensive calculation. The framework thus offers a cheap pre-screen for the ongoing experimental effort to identify HCI optical-clock transitions across isoelectronic sequences and charge states, complementing rather than replacing the ab initio treatment.

https://doi.org/10.3390/atoms14070060

5. Conclusions

We have developed a thresholded power-law scaling model $\Delta E = A(Z - Z^*)^\gamma$ for HCI low-lying level splittings and applied it to fourteen isoelectronic sequences covering valence shells from $2p$ to $4d$. Comparing the fitted threshold Z^* against the classical Slater shielding constant σ_{Slater} of the valence shell separates three distinct regimes: (i) Coulomb-LS sequences (C/N/O/Ne-like) with Z^* fixed at zero by construction; (ii) a fine-structure mainstream cluster of nine sequences for which Z^* tracks σ_{Slater} within ± 1.5 units; and (iii) a pair of $nd^6\ ^5D_0$ outliers—Cr-like $3d^6$ [6] and Mo-like $4d^6$ [5]—with $\Delta = Z^* - \sigma_{\text{Slater}} = +7.20$ and $+10.36$, respectively, well outside the bootstrap uncertainty.

The two members of the $nd^6\ ^5D_0$ pair are independent in computational origin, scale linearly with Z in the thresholded form, and exhibit a slope ratio $A_{\text{Mo}}/A_{\text{Cr}} \approx 0.48$ that is of the order of the hydrogenoid radial-extent ratio $\langle r^2\rangle(3d)/\langle r^2\rangle(4d) \approx 0.32$, exceeding it by $\sim$50% as expected from relativistic $4d$ contraction. Based on this consistency, we offered a falsifiable extrapolation for W-like $5d^6\ ^5D_0$: $\Delta \in [+7, +11]$, $A_W \in [0.12, 0.18]$ eV/Z, $Z^*_W \approx 78$, yielding clock-transition predictions rising to ≈ 2 eV (U-XXIII) for the upper-Z members above threshold ($Z \gtrsim 79$).

The broader picture from [1,6] and the present work is that the periodic table contains statistical regularities—Zipf-like in neutral atoms, thresholded-Zipf in HCIs—that survive across distinct ionization regimes provided the correct scaling coordinate is chosen. The diagnostic $\Delta = Z^* - \sigma_{\text{Slater}}$ then classifies sequences by whether classical screening or relativistic jj redistribution dominates. Whether the $nd^6\ ^5D_0$ regime extends to a third row of the periodic table is the immediate empirical question raised by this work.

Supplementary Materials: The following supporting information can be downloaded at: https://www.mdpi.com/article/10.3390/atoms14070060/s1, A supplementary table (Table S1) lists, for every sequence, the lower and upper levels (configuration, term, J) that define the fitted low-lying level splitting—term separation or fine structure—with the source for each. (Table S2) which presents the digitized Mo-like $4d^6\ ^5D_0$ excitation energies ΔE from Figure 2(b) of Lyu et al. reg." marks each point as belonging to the LS–jj crossover (cx, $Z < 58$) or the jj-linear regime (jj, $Z \geq 58$). The following supporting information can be downloaded as a single archive (`zipf_hci_paper_pack.tar.gz`) and will be archived on Figshare (DOI: *10.6084/m9.figshare.33022928*). The archive contains the SQLite database `hci_data_v4.db` (398 ions, 19,096 levels), JSON files of per-sequence fits, the YAML claims file used as single source of truth, and Python analysis scripts (`slater_shielding.py`, `thresholded_fit.py`, `reproduce_table1.py`, `reproduce_fig1.py`, `reproduce_fig2.py`).

Author Contributions: Conceptualization, A.F.F.d.S., S.D.S. and G.F.C.; methodology, A.F.F.d.S., R.M. and G.F.C.; software, A.F.F.d.S.; validation, A.F.F.d.S., R.M. and G.F.C.; formal analysis, A.F.F.d.S. and R.M.; investigation, A.F.F.d.S.; resources, A.F.F.d.S. and R.M.; data curation, A.F.F.d.S. and G.F.C.; writing—original draft preparation, A.F.F.d.S.; writing—review and editing, all authors; visualization, A.F.F.d.S.; supervision, S.D.S., R.M. and G.F.C. All authors have read and agreed to the published version of the manuscript.

Funding: This research was funded by CNPq and CAPES. The APC was funded by UFSC. This study was financed in part by the Coordenação de Aperfeiçoamento de Pessoal de Nível Superior—Brasil (CAPES Finance Code 001). G.F.C. thanks CNPq for a research scholarship (grants: 311132/2020-0 and 310550/2023-8)

Data Availability Statement: The full SQLite database (398 ions, 19,096 levels), Python analysis scripts including the digitization pipeline for Figure 2b of [5], the per-sequence fit results in JSON format, and the YAML claims file used as single source of truth for the numerical claims in this manuscript are available as Supplementary Material and on Figshare. The original $3d^{2+}$ dataset and code from the predecessor analysis [6] are available through the corresponding Figshare repository.

Acknowledgments: The authors thank the Brazilian government agencies CNPq, FAPESC, and CAPES. The authors thank the developers and curators of the NIST Atomic Spectra Database and of evaluated spectral compilations that make systematic atomic-structure studies possible. The authors also acknowledge the GRASP2018 developers, whose code provides the methodological backbone for testing the W-like prediction presented in Section 4.6.

Conflicts of Interest: The authors declare no conflicts of interest.

Note

[1] An "X-like" sequence is defined by the electron number of neutral X. The sequence of X-like *ions* begins at the first member for which the target fine-structure transition is well defined and evaluated. For Ne-, Ca-, and Sr-like sequences, this is the first ion ($Z = Z_X + 1$); for C-, N-, and O-like sequences, the neutral itself provides it, so the sequence starts at $Z = Z_X$.

References

1. Da Silva, S.; Matsushita, R.; Silva, M. A power law in the ordering of the elements of the periodic table. *Phys. A Stat. Mech. Its Appl.* **2020**, *548*, 123408. [CrossRef]
2. Kozlov, M.G.; Safronova, M.S.; Crespo López-Urrutia, J.R.; Schmidt, P.O. Highly charged ions: Optical clocks and applications in fundamental physics. *Rev. Mod. Phys.* **2018**, *90*, 045005. [CrossRef]
3. Safronova, M.S.; Budker, D.; DeMille, D.; Kimball, D.F.J.; Derevianko, A.; Clark, C.W. Search for new physics with atoms and molecules. *Rev. Mod. Phys.* **2018**, *90*, 025008. [CrossRef]
4. Lyu, C.; Keitel, C.H.; Harman, Z. Periodic table for highly charged ions. *Phys. Rev. Res.* **2025**, *7*, L042071. [CrossRef]
5. Lyu, C.; Keitel, C.H.; Harman, Z. Ultrastable and ultra-accurate clock transitions in open-shell highly charged ions. *Commun. Phys.* **2025**, *8*, 3. [CrossRef]
6. Da Silva, S.; Matsushita, R.; Caramori, G. From atoms to ions: Power-law scaling in the periodic table of highly charged ions. *J. Stat. Mech. Theory Exp.* **2026**, *2026*, 023204. [CrossRef]
7. Kramida, A.; Ralchenko, Y.; Reader, J.; NIST ASD Team. *NIST Atomic Spectra Database*, Version 5.12; National Institute of Standards and Technology: Gaithersburg, MD, USA, 2024. Available online: https://physics.nist.gov/asd (accessed on 1 April 2026). [CrossRef]
8. Sansonetti, J.E. Wavelengths, transition probabilities, and energy levels for the spectra of strontium ions (Sr II through Sr XXXVIII). *J. Phys. Chem. Ref. Data* **2012**, *41*, 013102. [CrossRef]
9. Sugar, J.; Musgrove, A. Energy levels of copper, Cu I through Cu XXIX. *J. Phys. Chem. Ref. Data* **1990**, *19*, 527–616. [CrossRef]
10. Sugar, J.; Musgrove, A. Energy levels of molybdenum, Mo I through Mo XLII. *J. Phys. Chem. Ref. Data* **1988**, *17*, 155–239. [CrossRef]
11. Kramida, A.; Shirai, T. Energy levels and spectral lines of tungsten, W III through W LXXIV. *At. Data Nucl. Data Tables* **2009**, *95*, 305–474. [CrossRef]
12. Slater, J.C. Atomic shielding constants. *Phys. Rev.* **1930**, *36*, 57–64. [CrossRef]
13. Bethe, H.A.; Salpeter, E.E. *Quantum Mechanics of One- and Two-Electron Atoms*; Springer: Berlin/Heidelberg, Germany, 1957.
14. Clementi, E.; Raimondi, D.L. Atomic screening constants from SCF functions. *J. Chem. Phys.* **1963**, *38*, 2686–2689. [CrossRef]
15. Jönsson, P.; Gaigalas, G.; Bieron, J.; Fischer, C.F.; Grant, I.P. New version: GRASP2018 – A Fortran 95 version of the General Relativistic Atomic Structure Package. *Comput. Phys. Commun.* **2019**, *237*, 184–187. [CrossRef]

Disclaimer/Publisher's Note: The statements, opinions and data contained in all publications are solely those of the individual author(s) and contributor(s) and not of MDPI and/or the editor(s). MDPI and/or the editor(s) disclaim responsibility for any injury to people or property resulting from any ideas, methods, instructions or products referred to in the content.